PUBLICATIONS OF THE ASTRONOMICAL SOCIETY OF THE PACIFIC, **115**:495–501, 2003 April

Astronomical Observing Conditions at the Xinglong Station in 1995–2001

YING LIU,[1] XU ZHOU,[1] WEI-HSIN SUN,[2] JUN MA,[1] HONG WU,[1] ZHAOJI JIANG,[1] SUIJIAN XUE,[1] AND JIANSHENG CHEN[1]
Received 2002 December 11; accepted 2003 January 13

ABSTRACT. This paper summarizes the measurements of astronomical observing conditions with a fixed pointing to the North Pole over 6 years at the Xinglong Station, where the BATC Multicolor Sky Survey has been conducted since 1995. Three major effects that influence the sky quality the most have been studied: the atmospheric transparency, the sky brightness, and the seeing. No obvious annual variation of the transparency was detected, but seasonal changes on a regular basis have been observed. The transparency is better and more stable in the winter than in the summer, which points to the fact that winter is the season for precise photometric work in Xinglong. The relations of sky brightness versus lunar phase and versus lunar altitude are derived and discussed. We find, on average, that the value of sky brightness in moonlight-corrected *V* magnitude of the North Pole field is about 21.0 mag arcsec^{-2}. The sky is darker in the fall and winter than in the spring and summer, and the transparency is better. It is conjectured that there are fewer particles in the air in the winter, thus both absorption and scattering are minimal. The seeing in the winter is worse than in the summer. This is probably due to the gusty wind from the northwest in the winter. The results of the North Pole monitoring presented in this paper show that the Xinglong Station is an astronomically good observing site. The North Pole observations will continue as a part of the BATC sky survey.

1. INTRODUCTION

The sky quality is vital to astronomical observations. Models have been constructed to predict the sky brightness caused by city light for certain sites (Garstang 1989), and the long-term periodic variations in seeing have been explored (Teare & Thompson 2002). In addition, numerous photometric observations have been obtained for a number of observatories to examine the sky quality and its temporal behavior as the surrounding natural and artificial environment evolves (Massey, Gronwall, & Pilachowski 1990). Here we generate a simple approach to evaluate the sky quality and its variation over a period of 6 years at the Xinglong Station for our Multicolor Sky Survey.

The Beijing-Arizona-Taipei-Connecticut (BATC) Sky Survey has been carried out at the Xinglong Station of the National Astronomical Observatories in China (NAOC) since 1995. The Xinglong station is located 170 miles northwest to Beijing at a longitude of $7^h50^m18^s$ east, a latitude of 40°23′36″ north, and an altitude of 950 m. It is the major optical/IR site for astronomical observations in China. In order to better understand Xinglong's observing conditions, including the atmospheric transparency, the sky brightness, and the seeing, we obtain wide-field photometry of the North Pole in every observable night. As a special target field in the survey, the North Pole has been imaged in BATC *i* band regularly since 1995. The accumulated information allows us to probe the periodic behavior in the sky condition parameters. In this article, we present the results over 6 years on the variation of these parameters and the correlations among them. The relations of the sky brightness versus the lunar phase and versus the lunar altitude are also addressed.

This article consists of four sections: § 1 gives an introduction; § 2 describes the photometric system of the BATC Sky Survey; § 3 presents the methodology of sky quality evaluation; § 4 contains the discussion and conclusions.

2. THE OBSERVATION OF THE NORTH POLE FIELD AND STANDARD STARS

The BATC Sky Survey produces wide-field photometry in a large range of optical wavelengths, using a Schmidt telescope of aperture 60/90 cm and a combined ratio of f/3. A Ford Aerospace 2048 × 2048 CCD with 15 μm pixels is mounted at the prime focus of the telescope. The field of view of this CCD camera is 58 × 58 arcmin^2 with a plate scale of 1.″7 pixel^{-1}.

The BATC Survey employs 15 intermediate-band filters, covering a wavelength range of 3000 to 10000 Å (Fan et al. 1996; Zhou et al. 2003). The filters are specifically designed to avoid contamination from most of the strong and variable night sky emission lines. The filter transmission parameters are tabulated in Table 1.

The BATC system adopts the AB_ν magnitude system of Oke & Gunn (1983). The advantage of the AB_ν system is that the

[1] National Astronomical Observatories, Chinese Academy of Sciences, Beijing 100012, People's Republic of China; liuying@vega.bac.pku.edu.cn.

[2] Institute of Astronomy, National Central University, Chung-Li 32054, Taiwan; sun@jade.astro.ncu.edu.tw.

TABLE 1
CENTRAL WAVELENGTHS AND EFFECTIVE BANDPASSES OF THE 15 BATC FILTERS

Number	Filter	Wavelength (Å)	Bandpass (Å)
1	*a*	3372.1	337.85
2	*b*	3895.3	266.65
3	*c*	4202.4	282.07
4	*d*	4547.4	355.53
5	*e*	4873.3	347.12
6	*f*	5248.4	331.49
7	*g*	5784.7	271.67
8	*h*	6074.3	289.77
9	*i*	6710.8	497.00
10	*j*	7011.3	170.62
11	*k*	7527.5	191.91
12	*m*	8025.4	260.27
13	*n*	8518.2	185.40
14	*o*	9173.8	269.48
15	*p*	9724.7	278.20

magnitude is directly related to the physical units. The magnitudes of the BATC system are defined as follows:

$$m_{\rm BATC} = -2.5 \log \tilde{F}_\nu - 48.60, \quad (1)$$

where $\tilde{F}_\nu$ is the flux per unit frequency in units of ergs s^{-1} cm^{-2} Hz^{-1} (Fan et al. 1996; Yan et al. 2000).

In the BATC system (Yan et al. 2000; Zhou et al. 2001), $\tilde{F}_\nu$ is defined as

$$\tilde{F}_\nu = \frac{\int d(\log \nu) f_\nu R_\nu}{\int d(\log \nu) R_\nu}, \quad (2)$$

where R_ν is the system response. This definition ties the magnitude directly to the number of photons detected rather than to the input flux (Fukugita et al. 1996). The system response R_ν used to relate f_ν and $\tilde{F}_\nu$ includes only the filter transmissions. Other effects such as the quantum efficiency (QE) of the CCD, the response of the telescope optics, and the atmospheric transmission, are relatively unimportant and can be ignored, due to the fact that the narrowness of the filter bandwidths makes most of these responses essentially flat within each band. Thus, the BATC system is basically filter-defined.

In every observable night, the field of the North Pole is observed at least once for the assessment of sky quality. The Schmidt telescope points to the real North Pole (decl. = 90°) with Polaris just outside of the field. The imaged area, centered on the real North Pole, effectively rotates relative to Polaris when taken at different time. The advantage of observing the North Pole lies in the fact that it is available all year for the Northern Hemisphere observatories at the same air mass with almost the same group of stars, making the derivation and comparison of sky quality parameters relatively simple and straightforward. The BATC *i* band filter, centered at 6660 Å with a bandwidth of 480 Å, is used in the observation. A short exposure is enough to achieve the goal of sky quality assessment. Thus, the exposure time is set to 100 s.

Usually a North Pole image is taken at the beginning of each night. In some cases, a second observation is obtained during the night for comparison. From 1995 March to the preparation of this manuscript, there have been a total of 1024 North Pole images collected in 978 observable nights, which were of different sky qualities.

In the nights considered photometric by the on-duty observers, two or more standard stars in addition to the program fields are observed repeatedly between air mass 1 and 2 in four to six selected filters. To save read-out time and storage space, only the central 300 × 300 region of the CCD is used. We first perform aperture photometry on these standard star images. To include as much flux as possible, an aperture radius of 15 pixels (about 25″) is selected. The extinction coefficient and instrumental zero point derived from these standard observations are then used for the subsequent flux calibration for all the program fields, including the North Pole observations (Zhou et al. 2001).

3. METHODOLOGY OF SKY QUALITY EVALUATION

3.1. Image Processing

Same as the processing of all the BATC images, the photometric data reduction of the North Pole images are first processed with the Source-Extractor software (Bertin et al. 1996). This software carries out the analysis of a CCD image in the following steps: estimating the sky background, thresholding, deblending, filtering of detections, obtaining photometry, classifying, and finally writing the results into an output catalog. The program is designed to find all the sources having maximum pixel value 3 σ above the sky background. For each source found, the output catalog lists its position in the image, the instrumental magnitude, the peak value in ADU, the adopted background value in ADU, and the FWHM of the sources in the images.

In the output catalog, we choose the ~100 brightest unsaturated stars for flux calibration and for the subsequent transformation from the BATC *i* magnitude to the standard broadband *V* magnitude. Since stars of different colors transform to *V* magnitude differently, we assumed a statistical approach and took average of the color indexes of these stars, to minimize the uncertainty in color transformations to a negligible level. After performing the astrometry sequence (Zhou et al. 2003), the equatorial coordinates of these stars are obtained, and their *V* magnitudes can be found in the Guide Star Catalogue (GSC). With this information, we can get the mean difference between the instrumental magnitudes and the *V* magnitudes of these stars.

One thing that needs caution is that for the North Pole ob-

servations, the 100 brightest unsaturated stars selected may not always be the same from image to image. This is due partly to the fact that the imaged area effectively rotates when taken at different times, thus a square CCD takes in different circumpolar stars at the four corners at different times. It is also due to the sky quality, which, if significantly better, would cause saturation and deletion of the top few brightest stars in a fixed exposure time (100 s).

The code POLESTAR was first developed for the assessment of the sky quality of the North Pole images on site. It was later generalized to apply to all BATC images at different pointings in various bands. It works as follows: the mean difference between the instrumental magnitudes of the selected stars in any two images of different BATC bands can be found. These differences among all the BATC bands can eventually be used to transform the instrumental magnitude of a particular band to *V* band. In addition, the mean atmosphere extinction in various BATC bands can be obtained from the observations taken in the photometric nights. With the corrections made to the magnitude, filter band, and the air mass, we can then derive the sky quality parameters (transparency, sky brightness, and seeing) and the limiting magnitude for every BATC image taken under different sky conditions in any BATC band.

However, in order to get a well-defined assessment of the sky quality and its periodic variations, we limit ourselves to the analysis of the North Pole monitoring images obtained during the 6 years from 1995 to 2001. The detailed description of the principles and techniques to obtain the sky quality parameters are given in the following sections.

3.2. Sky Transparency

Sky transparency is affected mainly by ozone molecule absorption and particle scattering in the atmosphere. The extinction coefficient at broadband *V*, K_V in mag per air mass, is usually adopted as an indicator of the transparency of an astronomical site. To obtain the transparency, we first write down the extinction equation:

$$m_{\rm inst} - m_{\rm BATC} = K \times {\rm AM} + C, \qquad (3)$$

where $m_{\rm inst}$ is the instrumental magnitude, $m_{\rm BATC}$ is the BATC magnitude for the filter, and AM is the air mass. The quantities *K* and *C* are the extinction at air mass of AM for the filter and that instrumental zero point, respectively. The quantity $m_{\rm inst}$ is defined as

$$m_{\rm inst} = -2.5 \log ({\rm ADU}) + 25.0. \qquad (4)$$

The definition of that magnitude system for the BATC Survey is based on the AB_ν system of Oke & Gunn (1983) (see eq. [1]). In particular, the filter used for the observations of the North Pole is centered at 6660 Å, which is the *i* band of the BATC system. Hence, equation (3) is transformed into

$$\overline{(m_{\rm inst})_i - m_V} = K_i \times {\rm AM} + C + D_{{\rm BATC}-V}, \qquad (5)$$

where

$$\overline{(m_{\rm inst})_i - m_V} = \sum_{n=1}^{100} \frac{[(m_{\rm inst})_i]_n - (m_V)_n}{100},$$

$$D_{{\rm BATC}-V} = \sum_{n=1}^{100} \frac{(m_{\rm BATC})_n - (m_V)_n}{100},$$

and $D_{{\rm BATC}-V}$ indicates the mean difference between BATC *i*-band magnitude and *V* magnitude of the 100 selected stars.

The instrumental magnitudes $(m_{\rm inst})_i$ can be measured directly from the images, and the values of m_V can be derived from the GSC. In order to get K_i for each observational night, we need to know *C* and $D_{{\rm BATC}-V}$. Since the instrumental zero point shows only long-term variations, but the change of extinction is primarily due to short-term effects, the change of instrumental zero point is thus negligible over short periods. The instrumental zero point *C* for each day can be interpolated among the measured values of standard stars obtained on photometric nights. The four standard stars used in flux calibration are from Oke & Gunn (1983): BD +17°4708, BD +26°2606, HD 84937, and HD 19445. We have observations of these four standard stars in a total of 33 photometric nights. These observations are used for the flux calibration of all BATC images including the North Pole observations. The instrumental magnitudes of standard stars at various air masses give the extinction curve. The extinction coefficient in the *i* band K_i and the instrumental zero point *C* can readily be derived from the extinction curve.

With K_i, *C*, and $\overline{(m_{\rm inst})_i - m_V}$ given, we can calculate $D_{{\rm BATC}-V}$ from equation (5). The North Pole images basically include the same group of stars all year, as discussed in the image processing section, so the group of 100 unsaturated stars remains approximately the same. Thus, the value of $D_{{\rm BATC}-V}$ remains constant with only a measurement error.

The extinction parameters from the photometric nights in which the North Pole field was also imaged are listed in Table 2. The first column in Table 2 is the Julian date of the night with only the last four digits shown. Columns (2), (3), and (4) are the instrumental zero point *C*, extinction coefficient K_i, and fitting error of extinction curves, respectively. The last column is $D_{{\rm BATC}-V}$ calculated by using equation (5).

From Table 2 we see that the variation of instrumental zero point *C* is fairly smooth over short timescales, which confirms empirically our assumption that *C* remains stable over short periods. This information allows the derivation of the instrumental zero point for every night in which the North Pole is imaged. From the observations made on photometric nights, we derived a mean $D_{{\rm BATC}-V}$ of 0.509 ± 0.012 mag. With in-

TABLE 2
EXTINCTION PARAMETERS OF THE NORTH POLE FIELD ON PHOTOMETRIC NIGHTS

Julian Date (1)	C (2)	Extinction K_i (3)	Error (4)	$D_{\mathrm{BATC}-V}$ (5)
9781	−0.378	0.196	0.030	0.522
9783	−0.313	0.119	0.011	0.506
9987	−0.426	0.099	0.004	0.541
9987	−0.426	0.099	0.004	0.525
0025	−0.554	0.334	0.017	0.493
0049	−0.596	0.337	0.019	0.583
0072	−0.559	0.109	0.005	0.490
0081	−0.503	0.101	0.003	0.494
0092	−0.378	0.110	0.005	0.454
0113	−0.411	0.070	0.011	0.479
0382	−0.691	0.120	0.006	0.452
0400	−0.613	0.109	0.003	0.469
0490	−0.458	0.096	0.009	0.461
0757	−0.489	0.127	0.005	0.488
0849	−0.658	0.135	0.011	0.486
0850	−0.714	0.232	0.009	0.562
1217	−0.783	0.111	0.010	0.463

terpolation we can estimate the instrumental zero point. Using the selected 100 stars, we can then get the value of $(m_{\mathrm{inst}})_i - m_V$. Thus, the extinction coefficient K_i for every night can then be found using equation (5).

The extinction coefficients for all 15 BATC bands, on the other hand, have been well studied, and a curve of the extinction versus wavelengths is given by Yan et al. (2000). With the information provided by Yan et al. (2000), we derive the statistical ratio between extinction coefficients at *i* band of 6660 Å and at *V* band of 5500 Å,

$$K_V = 1.9K_i. \tag{6}$$

Figure 1 shows the extinction coefficients K_V from 1995 to 2001. It is obvious that the fall and winter generally offer relatively more nights of better transparency than the spring and summer. From this figure, we estimate that the extinction coefficients for the best nights in fall and winter range from 0.1 to 0.3. The values are much higher and have more scatter in the summer.

3.3. Sky Brightness

The major contribution to the sky brightness is from atmospheric scattering of moonlight and city lights, in addition to the natural background from atmospheric emission at optical wavelengths. Since the Xinglong station is located in a remote area far from any sizable cities, the influence of city lights is insignificant. The moonlight then becomes a major factor to the sky brightness. The following analysis will then focus on the correlations between sky brightness and lunar phase and between sky brightness and lunar altitude.

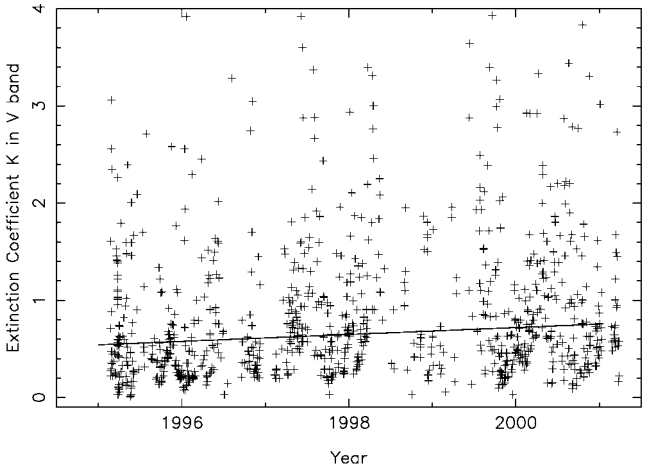

FIG. 1.—Variation of the atmospheric extinction coefficients from 1995 to 2001.

As has been performed in the derivation of extinction coefficient in the previous section, we obtain the relation between the instrumental magnitudes at *i* band and *V* magnitudes of the selected bright stars found in common in the North Pole survey images and in GSC. With a field of 1 arcsec^2 and relatively deep exposures of 1800 s, it is fairly straightforward to derive the sky brightness in ADU, which can readily be transformed into *V* magnitude for each survey image.

Since the moonlight contributes significantly to the sky brightness, we made an attempt to study the correlations between sky brightness and lunar phase and between sky brightness and lunar altitude, respectively. We overplot the measured sky brightness, which has been transformed into *V* magnitude, over the period of a month throughout 6 years in Figure 2. It

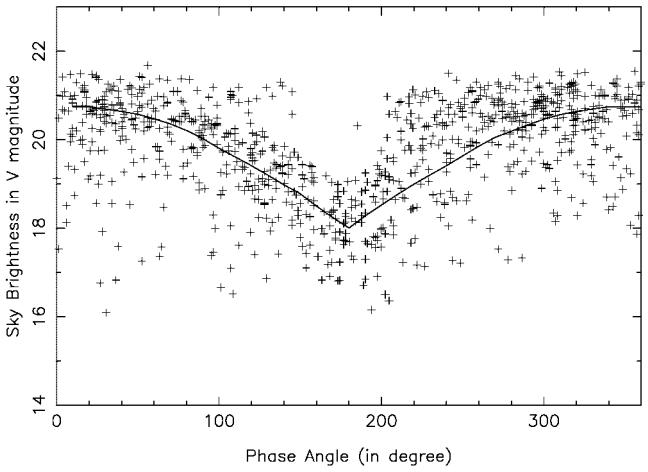

FIG. 2.—Least-squares fit to the variation of sky brightness as a function of lunar phase.

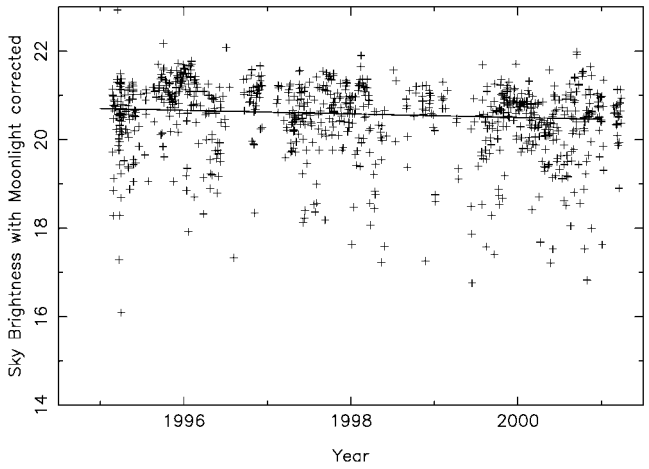

FIG. 3.—Variation of sky brightness from 1995 to 2001.

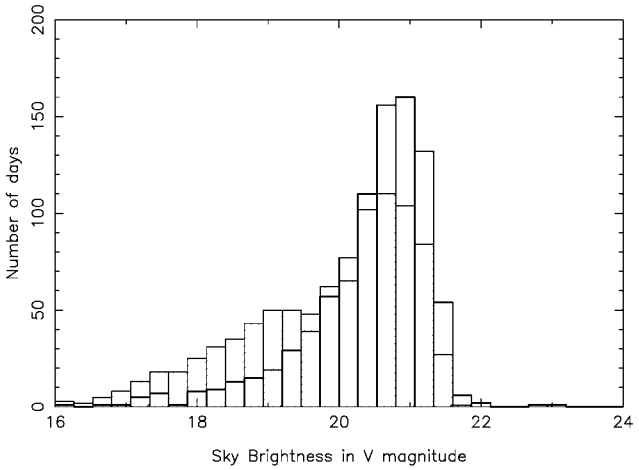

FIG. 4.—Histograms show the number of days as a function of sky brightness in 6 yr. The shaded area represents the original data, while the blank area indicates the moonlight effect corrected result.

is obvious that the sky brightness reaches the maximum when the Moon is full (at a phase angle of 180°).

The lunar phase can be expressed in terms of the Sun-Earth-Moon angle. An empirical formula describes the apparent V magnitude of the Moon as a function of Earth-Moon distance R and the Sun-Earth angle as seen from the Moon Φ (Zombeck 1990, p. 105):

$$V(R, \Phi) = 0.23 + 5 \log R - 2.5 \log P(\Phi), \quad (7)$$

where $P(\Phi)$ is the phase function for the Moon phase Φ, from 0 (new Moon) to 1 (full Moon). The value of $P(\Phi)$ can be read from Table 12.15 in *Allen's Astrophysical Quantities* (Cox 2000, p. 310).

Together with equation (4), we can see that the ADU value of the sky brightness is a linear function of $P(\Phi)$. We thus perform a least-squares fit to the ADU values for all nights and plot that data and the fit in Figure 2. The data points have also been corrected for the lunar altitude, which is explained in the following:

$$\mathrm{SB_{ADU}} = 56.975 + 546.318P(\Phi), \quad (8)$$

where $\mathrm{SB_{ADU}}$ is the sky brightness in ADU value with the lunar altitude corrected. Hence, we know from this equation that the sky brightness for the nights with full Moon is about 2.53 mag brighter than that in the nights with new Moon.

In addition to lunar phase, lunar altitude also contributes to the sky brightness, but with less influence compared to the change of lunar phase. The lunar altitude can easily be derived from the UT date in the observing log. It is an iterative process to derive the relations of sky brightness versus lunar phase and versus lunar altitude.

To demonstrate the influence of the lunar altitude, we fitted the sky brightness in V magnitude over the 6 years as a function of the lunar altitude from 0° to about 70°. The least-squares fit to the sky brightness as a function of lunar altitude gives the following relation:

$$\Delta \mathrm{SB}_V = -0.34 - 0.013A, \quad (9)$$

where $\Delta \mathrm{SB}_V$ is the sky brightness corrected for lunar phase and A is the lunar altitude in degrees.

The corrected sky brightness from 1995 to 2001 are plotted in Figure 3. It shows that the mean value of the sky brightness in 2001 is about 0.2 mag arcsec^{-2} brighter than in 1995. This is generally understood as being caused by the increasing solar activity in solar cycle 23, with its peak around 2000.

The histograms in Figure 4 show the distribution of days as a function of sky brightness in V mag over the 6 years. The shaded area represents the original data and the blank area indicates the sky brightness corrected for the moonlight effect, which is darker. With the moonlight effect removed, the values of sky brightness are concentrated between 20.5 and 21.5 mag arcsec^{-2} with a mean value of approximately 21.0 mag arcsec^{-2}.

To further investigate the correlation between the extinction coefficient and the sky brightness, a plot is made in Figure 5. A good linear relation can be found:

$$\mathrm{SB}_V = 21.11 - 0.924K_V, \quad (10)$$

where SB_V is the sky brightness in V magnitude and K_V is the extinction coefficient at broadband V.

This can be explained in terms of the abundance of molecules present in the atmosphere. The more molecules there are, the more absorption and scattering there is. The absorption manifests itself as atmosphere extinction, while the scattering dictates the sky brightness, when the effect of moonlight is prop-

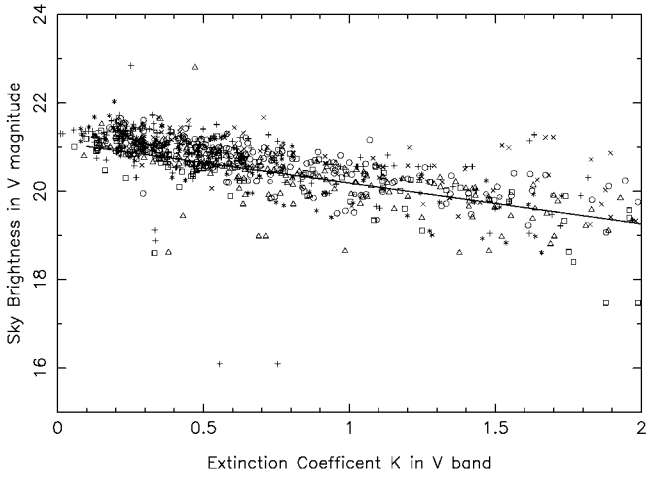

FIG. 5.—Correlation between the sky brightness in *V* magnitude and the atmospheric extinction of 6 yr.

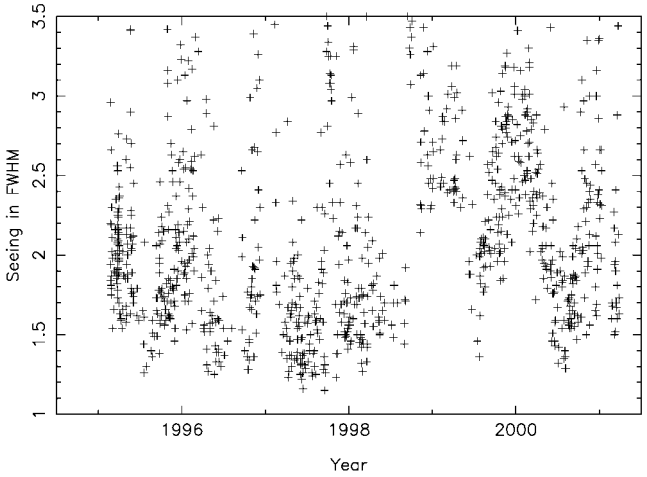

FIG. 6.—Variation of seeing from 1995 to 2001. Here we use FWHM (in pixels) for the seeing measure.

erly accounted for and removed. Thus, brighter background means lower transparency. It is reasonable to suspect that due to higher ground temperature, there could be more particles in the air during the spring and summer (for example, the gusty sandstorms in the Mongolia and Beijing area).

3.4. Seeing

Astronomical seeing, mainly caused by atmospheric turbulence, plays a crucial role in the detection and measurement of celestial sources. However, the precise measurement of the seeing is rather difficult, because the size of a star in an image is determined by the atmospheric turbulence, dome effect, and the optical structure along the light path in the telescope/detector system. In the BATC observing system, the plate scale on the CCD is $1\farcs7$ pixel^{-1}. The undersampling introduced by this low resolution would cause unreliable results if one measures only a single star by the traditional FWHM fitting. However, we introduce a simple method here to evaluate the periodic behavior of the seeing. We first choose a number of unsaturated bright stars in each image and perform Gaussian fit to derive their FWHM (in pixels). Then the mean FWHM of these stars is used as the indicator of the seeing. The variations of the mean FWHM thus give us a relatively objective estimate of the seeing conditions in Xinglong.

The result from the 6 years of observation is plotted in Figure 6. It can be shown that the seeing in 1999 and 2000 was poorer than in other years. We conjecture that, at least in part, the rising solar activity plays a role in the atmospheric steadiness. Over the 6 years, there seems to be a similar yearly pattern that duplicates itself from year to year. We thus overplot the 6 years of data as a function of the months in a year to see the seasonal variation (Fig. 7).

It is somewhat surprising to see that, despite the lower atmosphere transparency and higher sky background, the summer offers relatively better seeing cconditions. This can be partially explained in terms of the weather pattern in the Beijing area. During the winter, it is usually very cold and dry with many windy days. The gusty wind comes from the northwest and causes worse seeing. In the summer, a warm wind comes from the southeast ocean, and the flow of air is relatively more stable. Thus, in the summer the weather is warm and humid, and there are fewer windy days. The obvious contrast gives rise to significantly different pattern of turbulence over the Xinglong station.

To study the importance of the weather pattern contributing to the seeing, we have also considered dome effect and the thermal heating from the living and working area nearby. We performed tests on winter nights, taking star images at the zenith and also in the four directions in the dome. No obvious differences in star size are found in these images. Thus, we

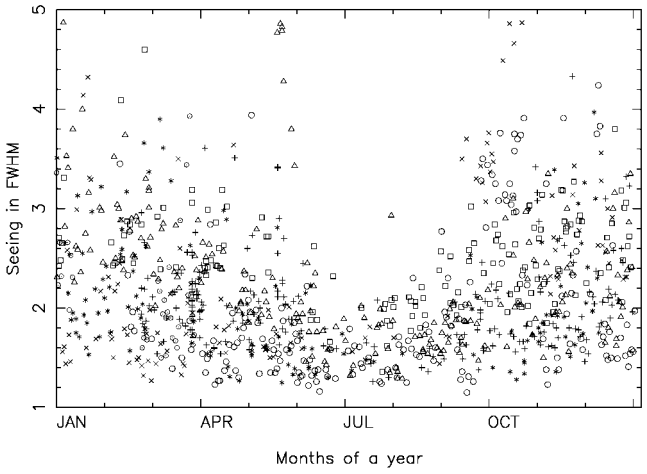

FIG. 7.—Seasonal variation of seeing over 6 yr.

can safely conclude that the seasonal variation of the seeing in Xinglong is mainly due to the seasonal wind, not to the local heating sources.

4. CONCLUSIONS

The North Pole region has been observed repeatedly with the BATC wide-field photometric system on every observable night since 1995, for the purpose of monitoring the sky quality over a long period of time. The abundance of data allows us to perform statistical analysis on the atmospheric extinction, moonlight effect, and seeing in Xinglong. In this paper, we present the results derived using data collected over 6 years from 1995 to 2001. Standard procedures have been developed and applied to the data to derive the extinction coefficients and the sky brightness in BATC magnitudes, which were subsequently transformed into *V* magnitudes using empirical conversion factors. The mean FWHM of stars in an image is used as a seeing indicator. Seasonal as well as annual variation of the extinction coefficient, sky brightness, and seeing have been studied. The average value of extinction K_V over 6 years is approximately 0.5 ± 0.2 mag per air mass. No obvious annual variation was detected, but seasonal changes on a regular basis have been observed.

The atmospheric transparency is better and more stable in the fall and winter than in the spring and summer, which leads us to conclude that fall and winter are the seasons for precise photometric work in Xinglong.

One major contribution to the sky brightness comes from moonlight. The relations for sky brightness versus lunar phase and versus lunar altitude are derived. After the moonlight contribution is properly accounted for and removed, the data can be used for the study of seasonal and annual variation of sky brightness over 6 years. We find that, on the average, the value of sky brightness in moonlight-corrected *V* magnitudes is about 21.0 mag arcsec^{-2}, compared with the sky brightness of 21.9 mag arcsec^{-2} on 1988 February 18, a night of fairly low solar activity at Kitt Peak (Massey, Gronwall, & Pilachowski 1990). The sky is darker in the winter in general. However, the sky brightness has increased by 0.2 mag in *V* band, from 1995 to 2001. This is explained in terms of the rising solar activity in solar cycle 23.

The seeing, on the other hand, varies with a larger amplitude on the timescale of a year. Obvious seasonal variation is also detected. Due to the prevailing gusty wind from the northwest bringing in cold and turbulent air in the winter, the seeing in Xinglong is worse than in the summer when a southeast wind prevails.

We have obtained parameters for the atmospheric transparency, sky background, and seeing, which all influence sky quality for astronomical observation to a certain degree. From the statistics, Xinglong has better transparency, darker sky, but worse seeing in the winter nights. On the other hand, the transparency and sky background all become worse but seeing remains acceptable in the summer. This is fortunate because most of the clear and observable nights are from September to February.

The results of this paper show that the Xinglong station is an astronomically good observing site, compared with the major international sites. The North Pole observations will continue as a part of the BATC sky survey. The results and analysis of this long-term monitoring will provide a good reference for observations made in Xinglong and a good comparison for other observing sites.

The BATC Survey is supported by the Chinese Academy of Sciences, the Chinese National Natural Science Foundation, under contracts 19833020 and 19503003. We also thank the assistants who helped with the observations for their hard work and kind cooperation. The authors thank Yu Lu for stimulating and helpful discussions. Wei-Hsin Sun thanks the Taiwan National Science Council for support under grant NSC 89-2112-M-008-021.

REFERENCES

Bertin, E., & Arnous, S. 1996, A&AS, 117, 393
Cox, A. N. 2000, Allen's Astrophysics Quantities (New York: AIP)
Fan, X., et al. 1996, AJ, 112, 628
Fukugita, M., Ichikawa, T., Gunn, J. E., Doi, M., Shimasaku, K., & Schneider, D. P, 1996, AJ, 111, 1748
Garstang, R. H. 1989, PASP, 101, 306
Massey, P., Gronwall, C., & Pilachowski, C. A. 1990, PASP, 102, 1046
Oke, J. B., & Gunn, J. E. 1983, ApJ, 266, 713
Teare, S. W., & Thompson, L. A. 2002, PASP, 114, 125
Yan, H., et al. 2000, PASP, 112, 691
Zhou, X., Jiang, Z., Xue, S., Wu, H., Ma, J., & Chen, J. 2001, Chinese J. Astron. Astrophys., 1, 372
Zhou, X., et al. 2003, A&A, 397, 361
Zombeck, M. V. 1990, Handbook of Space Astronomy and Astrophysics (Cambridge: Cambridge Univ. Press)